Molecular Crystals and Liquid Crystals
Publication details, including instructions for authors and subscription information:
http://www.tandfonline.com/loi/gmcl20

Ruthenium Complex with Pyrene Antenna for DSSCs

Dong Min Chang [a] , Joo Young Kim [a] & Young Sik Kim [a b]
[a] Department of Information Display, Hongik University, Seoul, 121-791, Korea
[b] Department of Science, Hongik University, Seoul, 121-791, Korea
Version of record first published: 17 Sep 2012.

To cite this article: Dong Min Chang , Joo Young Kim & Young Sik Kim (2012): Ruthenium Complex with Pyrene Antenna for DSSCs, Molecular Crystals and Liquid Crystals, 567:1, 63-70

To link to this article: http://dx.doi.org/10.1080/15421406.2012.702386

Mol. Cryst. Liq. Cryst., Vol. 567: pp. 63–70, 2012

ISSN: 1542-1406 print/1563-5287 online
DOI: 10.1080/15421406.2012.702386

Taylor & Francis
Taylor & Francis Group

Ruthenium Complex with Pyrene Antenna for DSSCs

DONG MIN CHANG,[1] JOO YOUNG KIM,[1]
AND YOUNG SIK KIM[1,2,*]

[1]Department of Information Display, Hongik University, Seoul 121-791, Korea
[2]Department of Science, Hongik University, Seoul 121-791, Korea

In this study, we have compared the well known N3 dye and Ru(II) complex substituted with antenna group, such as two pyrenes of both site to bipyridine. Molecular orbital analysis confirmed that the LUMO and LUMO+1 are essentially delocalized over the dcbpy and the antenna ligand, respectively. The TD-DFT calculations showed that the complex with pyrene antenna had more panchromatic absorption spectra in the region above 400 nm compared to N3 dye. Moreover, the absorption bands around between 400 and 550 nm were red-shifted and increase molar extinction coefficients due to the antenna unit.

Keywords antenna; DFT; dye-sensitized solar cells (DSSCs); Ruthenium; TD-DFT

1. Introduction

Recently much attention has been focused on the dye-sensitized solar cells (DSSCs), as possible low-cost photovoltaic devices [1]. Performance and stability of DSSC devices have been studied and significantly developed over the past decade [2–4]. Among the components of DSSC, the sensitizer is a crucial element, which significantly influences on the power conversion efficiency as well as the stability of the device. Up to now, the record for DSSC efficiency was held by a polypyridyl ruthenium sensitizer (11%) in combination with a voltaic iodide/triiodide mixture as electrolyte [5]. However, the conversion efficiency of DSSCs is still lower than that of the silicon-based photovoltaic cells. To obtain a high conversion efficiency, optimization of the short-circuit photocurrent (Jsc) and open-circuit potential (Voc) of the cell is essential. The value of Voc depends on the edge of conduction band in TiO_2 and the redox potential of I-/ I3-, otherwise Jsc is related to the interaction between TiO_2 and the sensitizer as well as the absorption coefficient of the sensitizer [6]. Furthermore, Jsc is closely related to the metal-to-ligand charge transfer (MLCT) transition of immobilized dye molecules, which could be improved significantly by means of the enrichment electron-donating ability of the ancillary ligand [7].

In order to enhance power conversion efficiencies of DSSCs, it is imperative to design novel sensitizers that exhibit an enhanced molar extinction coefficient in combination with a red-shifted absorption band compared to standard $[Ru(dcbpy)_2(NCS)_2]$. Extension of the

*Address correspondence to Young Sik Kim, Department of Information Display, Hongik University, Seoul 121-791, Korea. E-mail: youngkim@hongik.ac.kr

π-conjugation of the ancillary ligand and/or the anchoring ligand can improve the spectral response of corresponding ruthenium sensitizers [8]. Therefore, efforts were recently made to increase the molar extinction coefficients of the ruthenium dyes in order to improve their light-harvesting ability. In this work, we designed a novel heteroleptic ruthenium complex [Ru(dcbpy)(dpbpy)$(NCS)_2$] with high π-conjugated bipyridine ligand with pyrene group as a weak donor. The density functional theory (DFT) and time-dependent density functional theory (TD-DFT) calculations were used to estimate the photovoltaic properties of the dyes [9]. Finally, we will suggest high performed dye sensitizer as a DSSC device.

2. Computational Methods

To gain insight into the factors responsible for the absorption spectral response and the conversion efficiency, we perform DFT and TD-DFT calculations on the ground state of the ruthenium dyes. This computational procedure allows us to provide a detailed assignment of the excited states involved in the absorption process. The geometries and energy levels of molecular orbital were calculated by the DFT method and the absorption spectrum was calculated at optimized ground state geometries by the TD-DFT method. Although, the energy levels of molecular orbital can predict the trend of energy gap in the absorption spectrum, their data do not exactly match in the absorption spectrum. Since the absorption process has time dependency, the absorption spectrum in this study originates from TD-DFT.

The geometries in the gas phase were optimized by the DFT method using the B3LYP/DGDZVP in the Gaussian 03 program package. Possible isomers of the ruthenium complex with pyrene were calculated by the DFT. Among conformations, the present conformation was the lowest energy conformation, which is optimized the molecular structure of the dyes in the gas phase. Electronic populations of the highest occupied molecular orbital (HOMO) and the lowest unoccupied molecular orbital (LUMO) were calculated to show the position of the localization of electron populations along with the calculated molecular orbital energy diagram.

TD-DFT calculations with B3LYP/DGDZVP level of theory were performed at the ground state optimized geometries by means of the C-PCM algorithm, as implemented in the G03 program package. Absorption spectrum was calculated at optimized ground state geometries for lowest 30 singlet-singlet excitations up to wavelength of 400 nm. The simulation of the absorption spectra was performed by a Gaussian convolution with fwhm = 0.26 eV.

3. Results and Discussion

The chemical structures of dyes studied herein are shown in Fig. 1. The [Ru(dcbpy)(dpbpy)$(NCS)_2$] was designed by adding the pyrene antenna as a heteroleptic ruthenium complex. To increase the power conversion efficiency, the pyrene antenna was designed for extension of the π-conjugation system and enrichment the electron-donating ability. The π-conjugation system and enrichment the electron-donating ability would lead to red- shifted, broadened absorption band and improve the MLCT [6–8]. Therefore, the [Ru(dcbpy)(dpbpy)$(NCS)_2$] is expected to better performance in Jsc than the [Ru$(dcbpy)_2(NCS)_2$]. DFT calculations were performed at a B3LYP/DGDZVP level for the geometry optimization of these dyes in order to obtain molecular orbitals and electronic structures of the [Ru$(dcbpy)_2(NCS)_2$] and the [Ru(dcbpy)(dpbpy)$(NCS)_2$].

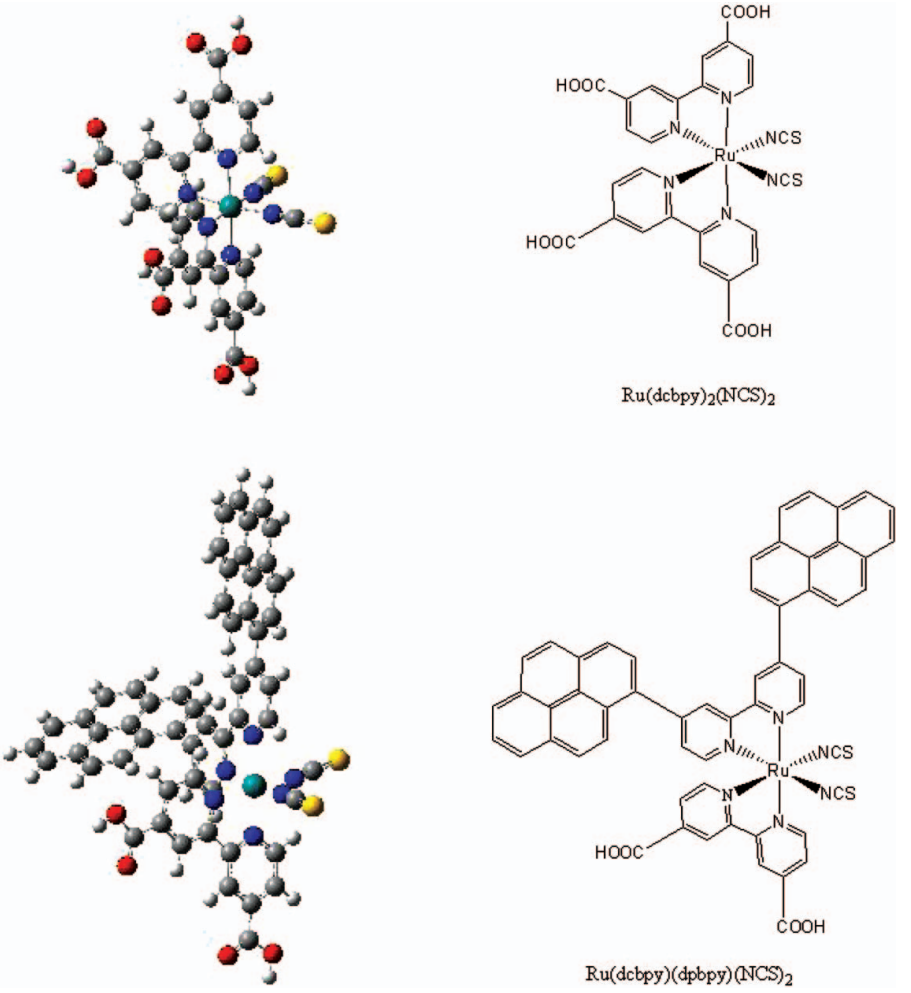

Figure 1. Molecular structure of the dyes: $[Ru(dcbpy)_2(NCS)_2]$ and $[Ru(dcbpy)(dpbpy)(NCS)_2]$.

These dyes with their isodensity surface plots of the frontier MOs are shown in Fig. 2. It shows that the HOMO orbitals of the $[Ru(dcbpy)_2(NCS)_2]$ are delocalized over the NCS groups. The HOMO, HOMO-1, HOMO-2, HOMO-3 of the $[Ru(dcbpy)(dpbpy)(NCS)_2]$ are delocalized over the NCS groups, on the other hand, HOMO-4 is mainly localized on pyrene moiety. In case of the $[Ru(dcbpy)_2(NCS)_2]$, LUMO orbitals are mainly localized on the dcbpy groups. In case of LUMO and LUMO+3 of the $[Ru(dcbpy)(dpbpy)(NCS)_2]$ are localized on the dcbpy groups, however, the LUMO+1, LUMO+2 and LUMO+4 of the $[Ru(dcbpy)(dpbpy)(NCS)_2]$ are delocalized on the pyrene moiety.

Fig. 3 shows the calculated molecular orbital energy diagram for these dyes. Overall, energy gaps between HOMOs and LUMOs levels of the $[Ru(dcbpy)(dpbpy)(NCS)_2]$ were decreased with additional pyrene group. Specifically, HOMOs levels (HOMO-3, HOMO-4) and LUMO+1 of the $[Ru(dcbpy)(dpbpy)(NCS)_2]$ were destabilized by the electron-donating characteristic of pyrene group. As shown in Fig. 2, the LUMO+1 of $[Ru(dcbpy)(dpbpy)(NCS)_2]$ was mainly localized on pyrene moiety. These results lead to

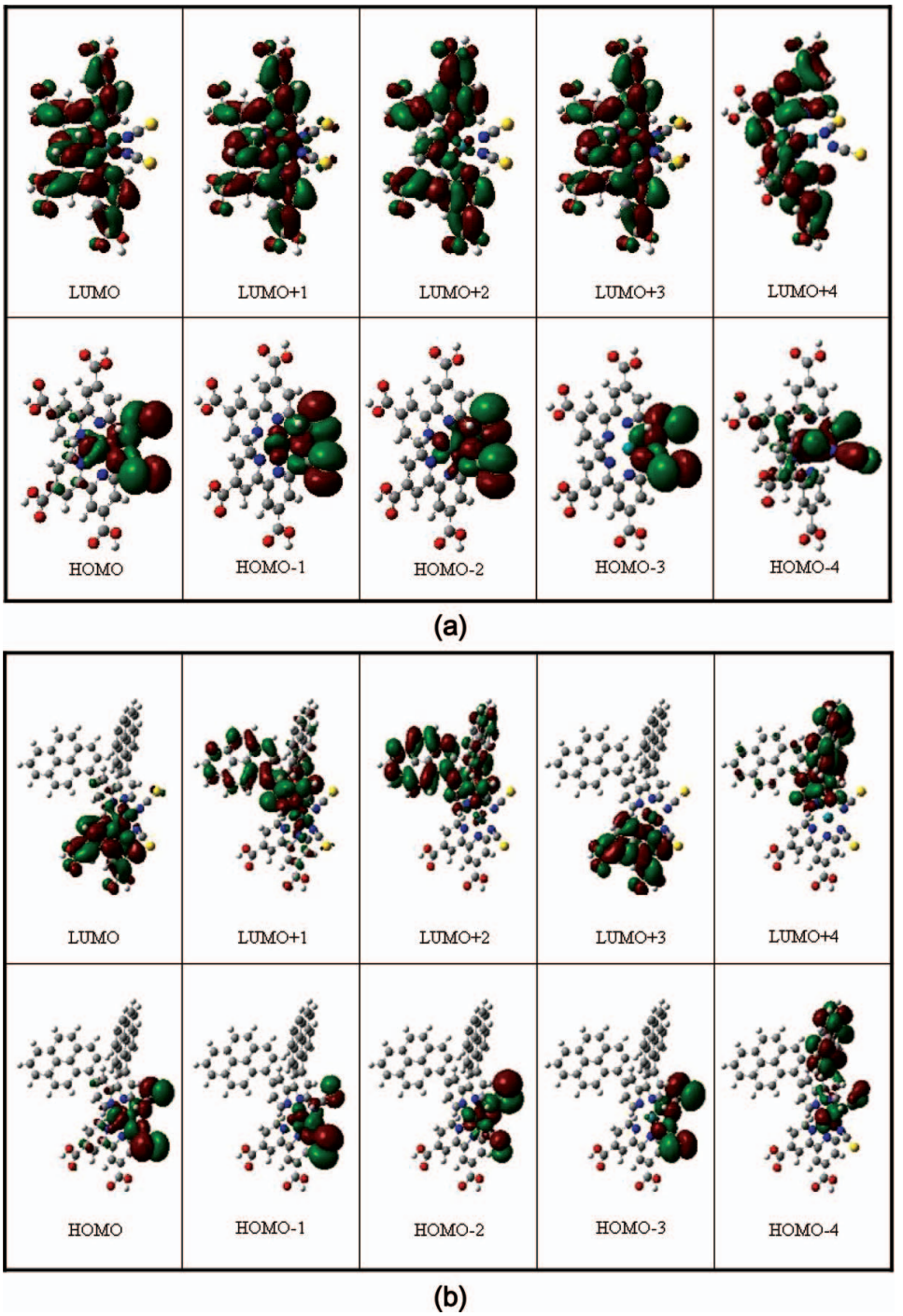

Figure 2. Frontier molecular orbitals (HOMOs, LUMOs): (a) $[Ru(dcbpy)_2(NCS)_2]$ (b) $[Ru(dcbpy)(dpbpy)(NCS)_2]$.

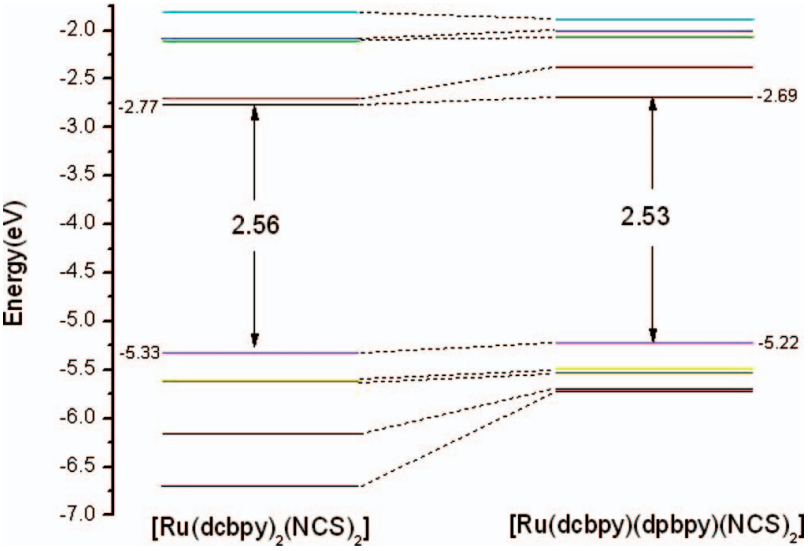

Figure 3. Schematic energy diagram for $[Ru(dcbpy)_2(NCS)_2]$ and $[Ru(dcbpy)(dpbpy)(NCS)_2]$.

the reduction of energy gaps between HOMOs and LUMOs levels when compared with that of the $[Ru(dcbpy)_2(NCS)_2]$. The reduction of the energy gap of the dye would show more red-shifted band in the absorption spectrum and panchromatic absorption band in the long wavelength region.

Figure 4 shows the UV-Vis absorption spectra of the $[Ru(dcbpy)_2(NCS)_2]$ and the $[Ru(dcbpy)(dpbpy)(NCS)_2]$ dyes by TDDFT calculations. Both the dyes show three

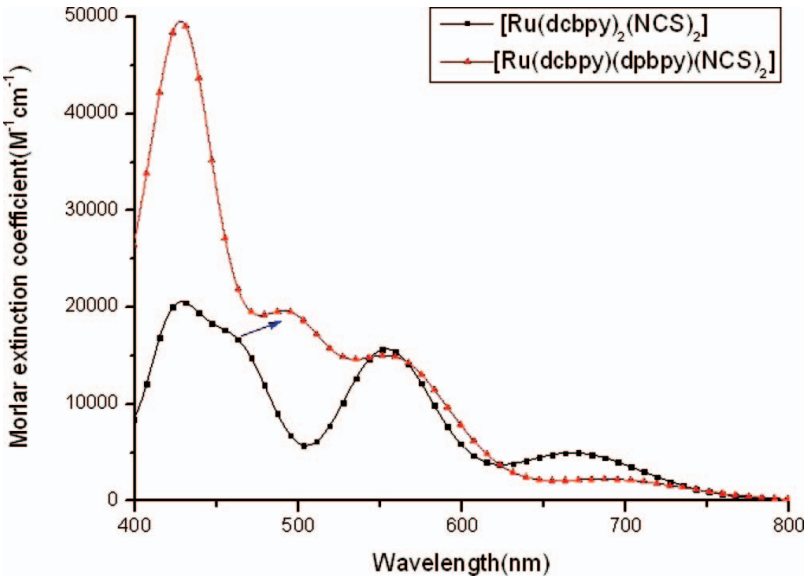

Figure 4. The calculated absorption spectra of the dyes: $[Ru(dcbpy)_2(NCS)_2]$ and $[Ru(dcbpy)(dpbpy)(NCS)_2]$.

Table 1. Calculated TDDFT excitation energies (eV, nm), oscillator strengths (f) and composition in terms of MO contributions: [Ru(dcbpy)$_2$(NCS)$_2$] and [Ru(dcbpy)(dpbpy)(NCS)$_2$]

Dye	# of excited state	Calculated energy(eV, nm)	strengh(f) Oscillator	Major composition
[Ru(dcbpy)2(NCS)2]	1	2.877 (430.94)	0.0195	H-1->L+3 (47%), HOMO->L+4 (50%)
	2	2.726 (454.83)	0.0355	HOMO->L+3 (72%)
	3	2.2302 (555.94)	0.1379	H-2->LUMO (51%), H-1->L+1 (39%)
[Ru(dcbpy)(dpbpy)(NCS)2]	1	2.8978 (427.86)	0.1242	H-3->L+1 (88%)
	2	2.4901 (497.9)	0.1418	H-2->L+1 (15%), H-1->L+1 (52%), HOMO->L+2 (17%)
	3	2.2444 (552.42)	0.1004	H-2->LUMO (71%), H-1->L+1 (6%), HOMO->LUMO (4%)

absorption bands of MLCT in visible region. The three absorption bands of the [Ru(dcbpy)(dpbpy)$(NCS)_2$] are centered at 428, 494 and 558 nm with the molar extinction coefficients of 4.95×10^4 $M^{-1}cm^{-1}$, 1.96×10^4 $M^{-1}cm^{-1}$ and 1.50×10^4 $M^{-1}cm^{-1}$, respectively, while the [$Ru(dcbpy)_2(NCS)_2$] presents three bands at 428, 458 and 554 nm corresponding 2.06×10^4 $M^{-1}cm^{-1}$, 1.72×10^4 $M^{-1}cm^{-1}$ and 1.56×10^4 $M^{-1}cm^{-1}$, respectively. For the [Ru(dcbpy)(dpbpy)$(NCS)_2$], the absorption intensity of high energy MLCT band is 2.4 times stronger than the corresponding value of the [$Ru(dcbpy)_2(NCS)_2$] and the second high energy MLCT band is red-shifted about 36 nm, with slightly increase of the molar extinction coefficient, while the low energy MLCT band is red-shifted about 4 nm when compared with that of the [$Ru(dcbpy)_2(NCS)_2$]. The red-shifted MLCT band is in agreement with the extension of π-conjugation of the pyrene moiety, which results in decrease between HOMOs and LUMOs levels. The absorption peaks at 428 nm, 458 nm and 554 nm of the [$Ru(dcbpy)_2(NCS)_2$] are mainly contributed from HOMO $\rightarrow$ LUMO+4, HOMO $\rightarrow$ LUMO+3 and HOMO-2 $\rightarrow$ LUMO transition, respectively (see Table 1). The absorption peak at 428, 494 and 558 nm of [Ru(dcbpy)(dpbpy)$(NCS)_2$] are mainly contributed from the HOMO-3 $\rightarrow$ LUMO+1, HOMO-1 $\rightarrow$ LUMO+1 and HOMO-2 $\rightarrow$ LUMO transition, respectively. Focused on the absorption band at 428 nm and 494 nm of [Ru(dcbpy)(dpbpy)$(NCS)_2$], these peaks are originated from the HOMO-3 $\rightarrow$ LUMO+1 (88%) and HOMO-1 $\rightarrow$ LUMO+1 (52%) transitions, respectively. As shown in Fig. 2 and Fig. 3, the LUMO+1 was delocalized over the pyrene moiety and HOMO-3 was destabilized by introducing pyrene. Therefore, the significantly increase of the molar extinction coefficients at 428 nm and the red-shifted absorption band from 458 nm to 494 nm are due to the introduction of pyrene as an ancillary ligand. Moreover, absorption energy bands of [Ru(dcbpy)(dpbpy)$(NCS)_2$] showed enhanced molar extinction coefficients between 400 nm and 550 nm in the visible light region, compared with [$Ru(dcbpy)_2(NCS)_2$], due to the π-conjugated bipyridine ligand with pyrene group as a weak donor.

It has been reported that the retardation in charge-recombination dynamics is related to the physical separation between dye-cation moiety and surface of the TiO_2 surface [10,11]. As shown in Fig. 1 and Fig. 2, the distance between the HOMO-4 of [Ru(dcbpy)(dpbpy)$(NCS)_2$] and the anchoring moiety is longer than that of [$Ru(dcbpy)_2(NCS)_2$]. This means that [Ru(dcbpy)(dpbpy)$(NCS)_2$] have longer charge-separated lifetime than [$Ru(dcbpy)_2(NCS)_2$]. In order to these results, [Ru(dcbpy)(dpbpy)$(NCS)_2$] would be expected high light-harvesting and conversion efficiency as a photovoltaic device.

4. Conclusions

Novel heteroleptic ruthenium complex with pyrene antenna was designed and studied theoretically for the potential devices of DSSCs. Specifically, structural, electronic and optical properties of the [Ru(dcbpy)(dpbpy)$(NCS)_2$] were investigated with the introduction to pyrene as an ancillary ligand. In electronically, HOMOs levels (HOMO-3, HOMO-4) and LUMO+1 were destabilized by the electron-donating characteristic of pyrene. The absorption spectra of the [Ru(dcbpy)(dpbpy)$(NCS)_2$] showed more broad and red-shifted by the additional pyrene antenna. Moreover, the molar extinction coefficients significantly increase between 400 nm and 550 nm. This means that the [Ru(dcbpy)(dpbpy)$(NCS)_2$] is expected to efficient light harvesting and better performance in J_{sc} than the [$Ru(dcbpy)_2(NCS)_2$]. Furthermore, due to the difference distance between the HOMO-4 and the anchoring moiety, [Ru(dcbpy)(dpbpy)$(NCS)_2$] would have longer charge-separated lifetime than [$Ru(dcbpy)_2(NCS)_2$]. Therefore, we suggest that newly

designed [Ru(dcbpy)(dpbpy)$(NCS)_2$] heteroleptic ruthenium complex would be a good candidate as a dye sensitizer of DSSCs, comparable to [Ru$(dcbpy)_2(NCS)_2$].

Acknowledgment

This research was supported by the Basic Science Research Program through the National Research Foundation of Korea (NRF) funded by the Ministry of Education, Science and Technology (2010–0021668).

References

[1] Baldo, B., Regan, O., & Grätzel, M. (1991). *Nature* (London), *353*, 737.
[2] Kuang, D., Ito, S., Wenger, B., Klein, C., Moser, J. E., Humphry-Baker, R., Zakeeruddin, S. M., & Grätzel, M. (2006). *J. Am. Chem. Soc.*, *128*, 4146.
[3] Kuang, D., Klein, C., Ito, S., Moser, J. E., Humphry-Baker, R., Zakeeruddin, S. M., & Grätzel, M. (2007). *Adv. Funct. Mater.*, *17*, 154.
[4] Kuang, D., Klein, C., Ito, S., Moser, J. E., Humphry-Baker, R., Evans, N., Duriaux, F., Grätzel, C., Zakeeruddin, S. M., & Grätzel, M. (2007). *Adv. Mater.*, *19*, 1133.
[5] Nazeeruddin, M. K., Angelis, F. D., Fantacci, S., Selloni, A., Viscardi, G., Liska, P., Ito, S., Takeru, B., & Grätzel, M. (2005). *J. Am. Chem. Soc.*, 127, 16835.
[6] Wang, P., Klein, C., Humphry- Baker, R., Zakeeruddin, S. M., & Grätzel, M. (2005). *Appl. Phys. Lett.*, *86*, 123508.
[7] Jheng-Ying, Li, Chia-Yuan, Chen, Jian-Ging, Chen, Chun-Jui, Tan, Kum-Mu, Lee, Shi-Jhang, Wu, Yung-Ling, Tung, Hui-Hsu, Tsai, Kuo-Chuan, Ho, & Chun-Guey, Wu, (2010). *J. Mater. Chem.*, *20*, 7158.
[8] Horiuchi, T., Miura, H., Sumioka, K., & Uchida, S., (2004). *J. Am. Chem. Soc.*, *126*, 12218.
[9] Tian, H., Yang, X., Cong, J., Chen, R., Liu, J., Hao, Y., Hagfeldt, A., & Sun, L., (2009). *Chem. Commun.*, 6288.
[10] Haque, S. A., H&a, S., Peter, K., Palomares, E., Thelakkat, M., & Durrant, J. R., (2005). *Angew. Chem., Int. Ed.*, *44*, 5740.
[11] Handa, S., Wietasch, H., Thelakkat, M., Durrant, J. R., & Haque, S. A., (2007). *Chem. Commun.*, 1725.